Editors' Suggestion | Featured in Physics

Ferroelectric Switchable Altermagnetism

Mingqiang Gu,[1] Yuntian Liu,[1,‡] Haiyuan Zhu,[1] Kunihiro Yananose,[2] Xiaobing Chen,[3] Yongkang Hu,[1] Alessandro Stroppa,[4,*] and Qihang Liu[1,3,5,†]

[1]Department of Physics and Guangdong Basic Research Center of Excellence for Quantum Science, Southern University of Science and Technology, Shenzhen 518055, China
[2]Korea Institute for Advanced Study, Seoul 02455, Republic of Korea
[3]Quantum Science Center of Guangdong–Hong Kong–Macao Greater Bay Area (Guangdong), Shenzhen 518045, China
[4]CNR-SPIN, Department of Physical and Chemical Sciences, University of L'Aquila, Via Vetoio, 67100 L'Aquila, Italy
[5]Guangdong Provincial Key Laboratory of Computational Science and Material Design, Southern University of Science and Technology, Shenzhen 518055, China

(Received 6 November 2024; accepted 14 February 2025; published 13 March 2025)

We propose a novel ferroelectric switchable altermagnetism effect: the reversal of ferroelectric polarization is coupled to the switching of altermagnetic spin splitting. We demonstrate the design principles for the ferroelectric altermagnets and the additional symmetry constraints necessary for switching the spin splitting through flipping the electric polarization based on the state-of-the-art spin-group symmetry techniques. We find 22 ferroelectric altermagnets by screening through the 2001 experimental reported magnetic structures in the MAGNDATA database and identify two of them as ferroelectric switchable altermagnets. Using the hybrid improper ferroelectric material $[C(NH_2)_3]Cr(HCOO)_3$ as an example, we show how the altermagnetic spin splitting is tightly coupled to the ferroelectric polarization, providing an ideal platform for designing electric-field-controllable multiferroic devices. Finally, we find that such manipulation of altermagnetism can be detected by monitoring the physical quantities that are related to the nonvanishing Berry curvature dipole, such as the linearly polarized photogalvanic spin current.

DOI: 10.1103/PhysRevLett.134.106802

Introduction—Multiferroic materials exhibit more than one type of ferroic order simultaneously, such as ferroelectricity (spontaneous electric polarization) and magnetism (ferromagnetism or antiferromagnetism) [1]. In particular, magnetoelectrically coupled multiferroic materials have attracted significant interest due to their potential for controlling magnetic properties through electric fields, and vice versa, opening pathways for innovative applications in memory storage, sensors, and spintronics [2–5]. Multiferroics are broadly categorized into two types [6]. In type-I multiferroics, ferroelectric and magnetic orders originate from distinct mechanisms [7,8], which often results in weak coupling between these order parameters. In contrast, type-II multiferroics demonstrate stronger coupling because ferroelectricity arises directly from magnetic ordering [9]. Historically, the design and manipulation of multiferroicity primarily rely on the interaction between net magnetic moments and electric polarization [10]. For example, in multiferroic antiferromagnet $Ca_3Mn_2O_7$, the multiferroic coupling stems from the ferroelectric polarization and the net magnetic moment induced by spin-orbit coupling (SOC), i.e., Dzyaloshinskii-Moriya interaction [11]. However, the small weak ferromagnetic (FM) magnetization (0.045 μ_B/Mn in theory and 0.0025 μ_B/Mn in experiment) [12] limits the strength of magnetoelectric coupling and thus the multiferroic applications.

Recently, altermagnetism has garnered considerable attention [13–16] as a promising avenue for achieving novel spintronic properties. Altermagnets are a class of collinear antiferromagnetic (AFM) materials characterized by alternating spin polarization across reciprocal space due to breaking of certain spatial symmetries, even though they have no net macroscopic magnetization. The order parameter S featuring altermagnetism can be represented by the energy splitting between the two spin channels in certain paths of the Brillouin zone $\Delta E_k^s = E_k^{\uparrow} - E_k^{\downarrow}$. The spin-split bands of Bloch electrons in altermagnets create the possibility of designing new types of spintronic devices, e.g., spin-filtering magnetic tunnel junctions [17,18]. Because of the combination of the advantages of FM and AFM in terms of spin splitting, altermagnetism is also considered a third type of collinear magnetism [14,19].

In this Letter, we introduce the "ferroelectric switchable altermagnets," a new class of unconventional magnets [20] that shows not only the coexistence of ferroelectricity and altermagnetism, but also the synergistic coupling of the two order parameters, leading to a reversal of spin character in

*Contact author: alessandro.stroppa@spin.cnr.it
†Contact author: liuqh@sustech.edu.cn
‡Present address: State University of New York at Buffalo, Buffalo, NY, USA.

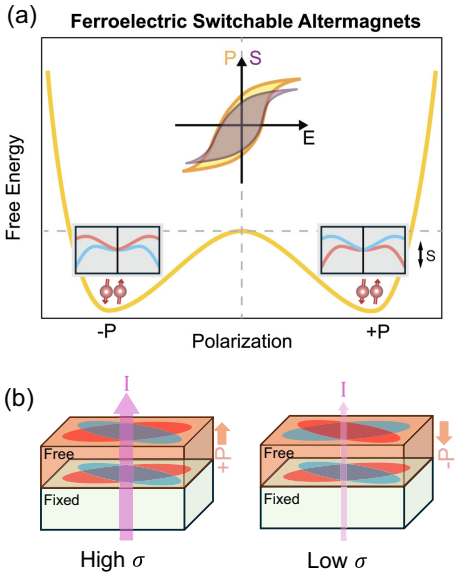

FIG. 1. (a) Schematic illustration of ferroelectric switchable altermagnetism, where the altermagnetic spin splitting S strongly couples to the ferroelectric polarization P. (b) A nonvolatile spin filtering tunnel junction device design with ferroelectric switchable altermagnets. The Fermi surfaces of the fixed layer and the free layer are also illustrated. The electric polarization P can be used to control the spin polarization of the free layer, leading to a transition between high- and low-conductance (σ) states.

split energy bands by switching the ferroelectric polarization. As illustrated in Fig. 1(a), in specific circumstances, the altermagnetic spin degree of freedom is tightly correlated to the electric polarization, indicating a distinct form of magnetoelectric coupling. Such a mechanism enables the control of a nonvolatile spin-split electronic dispersion through the external electric field, providing an efficient route to achieve robust all-in-one multiferroic memory devices. For example, Fig. 1(b) illustrates an electric-field-controllable spin-filtering altermagnetic tunnel junction device *without the need of switching the Néel vector*. By considering whether the spin-polarized Fermi surface between the free layer and the fixed layer match or not [14], the conductance σ can be switched between high and low by simply switching the ferroelectric polarization. By applying the state-of-the-art spin-group symmetry analyses, we searched through all the MAGNDATA database [21] and screened out 22 ferroelectric altermagnets, in which only two candidates support the synergistic switching of altermagnetic spin splitting through ferroelectric polarization.

We discuss a representative case, i.e., the metal-organic framework system (Cr-MOF), to showcase the ferroelectric switchable altermagnets. This material has been experimentally synthesized and theoretically proposed as a hybrid improper ferroelectric [22,23]. Here, we predict that the altermagnetic spin splitting in this material is tightly coupled to the ferroelectric polarization, in both the magnitude and the sign of ΔE_k^s, providing an ideal platform for spintronic devices. Finally, we find that the manipulation of altermagnetism can be monitored by the nonlinear optical generation of spin current, which originates from the nonzero Berry curvature dipole.

Material design principles—Altermagnetic spin splitting is a nonrelativistic property that manifests without the need for spin-orbit coupling, where the symmetry-theoretical framework should adopt the spin space group (SSG) [15,24–28] instead of the commonly used magnetic space group (MSG). We first consider ferroelectric altermagnets where the two order parameters P and S are not necessarily coupled. Two rules under the framework of SSG emerge: (i) for a collinear antiferromagnet manifesting spin splitting in the momentum space, the symmetries of joint parity and time reversal ($\mathcal{PT}$) and $\mathcal{T}\tau$, with τ being the fractional lattice translation, should be broken; (ii) for ferroelectric material, the spatial part of the parent space group (SG) of the SSG should belong to a polar group.

We diagnosed the SSGs of the 2001 experimentally reported magnetic structures in the MAGNDATA database by using our homemade online program FINDSPINGROUP [29], and found 22 systems that meet the above criteria. One immediately finds that the filtered materials can be divided into two classes by examining the MSG of the materials: the MSG of the first class allows spin canting, leading to a nonzero residual FM moment, while the second class forbids net magnetic moment in the system. For the first class with P-M coupling, the electronic polarization can interplay with the weak FM moment, leading to a classical magnetoelectric coupling [11]. Note that SOC plays an essential role (e.g., Dzyaloshinskii-Moriya interaction) in slightly tilting the spins from the collinear AFM configuration. For the second class without P-M coupling, since the net magnetic moment is forbidden by MSGs, the flipping of electric polarization is not supposed to induce any macroscopic effect on the magnetization. However, both classes are potential candidates for ferroelectric switchable altermagnets if the real-space electric polarization and the momentum-space spin splitting are coupled, even without SOC.

In general, the coexistence of electric polarization P and altermagnetic spin splitting ΔE_k^S (denoted by S) does not guarantee their coupling. Therefore, we next focus on the search of symmetry operations that synergistically switch P and S, and if these operations correspond to reasonable flipping paths under an external electric field, which does not change the Néel order. For example, considering an initial state $\psi_k^i(P,S)$, one can always flip both electric and spin polarization by applying a joint operation $\mathcal{PT}$ to the system to get a reversed state $\mathcal{PT}\psi_k^i(P,S)=\psi_k^f(-P,-S)$. However, in the transition path connecting $\psi_k^f(-P,-S)$ and $\psi_k^i(P,S)$ phases, the Néel vector may also be reversed, indicating a transition path that cannot be achieved by

electric field only. By going through the list in Table SI in Supplemental Material Sec. I [30], we found that the sign of ΔE_k^S for most candidates remains unchanged during the polarization reversal, as exemplified by $PbNiO_3$ (see Supplemental Material Sec. II [30]). Interestingly, there are two hybrid improper ferroelectric materials, $Ca_3Mn_2O_7$ and $[C(NH_2)_3]Cr(HCOO)_3$, as prototypical candidates of ferroelectric switchable altermagnets.

Altermagnetism in hybrid improper ferroelectric Cr-MOF—Hybrid improper ferroelectricity arises from a combination of two or more lattice modes that individually preserve inversion symmetry but collectively break it, resulting in a spontaneous polarization. Several candidate materials from Class 1 in Table SI [30] belong to this category, including $Ca_3Mn_2O_7$ (SG $Cmc2_1$) [43] and the hybrid organic-inorganic perovskite $[C(NH_2)_3]M(HCOO)_3$ (SG $Pna2_1$) with M being transition-metal elements Cu or Cr. Below we use Cr-MOF [see Fig. 2(a)] to illustrate the design principles of ferroelectric switchable altermagnets for two reasons: (a) it exhibits a large spin splitting near the Fermi level, and (b) various AFM configurations can be realized in Cr-MOF through compressive strain, offering an additional degree of freedom for phase manipulation [44]. Here, we focus on the C-type configuration, as it manifests large spin splitting. Further discussions on other metal-organic frameworks and AFM configurations can be found in Supplemental Material Sec. III [30].

The spin-polarized band structure obtained from density-functional theory (see Supplemental Material Sec. IV [30]) calculations is shown in Fig. 2(b). The band gap is about 3 eV, ensuring a good insulating background that is favorable for ferroelectrics. Notably, a large spin splitting is observed at the valence band maximum, with the largest energy difference being approximately 20 meV. Such spin splitting occurs at the relatively low-symmetry points in reciprocal space, such as along the $\Gamma(0,0,0) \rightarrow R(0.5,0.5,0.5)$ path. The spin-polarized isoenergy contour at $E = -0.05$ eV is shown in Fig. 2(c), showing a deviated feature compared with the so-called "d-wave" altermagnetism because of the absence of fourfold symmetry. Furthermore, the sign of ΔE_k^S, a well as the spin polarization of a given spin-polarized band, are odd under mirror operations $\{1\|m_{100}\}$ and $\{1\|m_{010}\}$, and even under $\{1\|m_{001}\}$, as illustrated in Fig. 2(e).

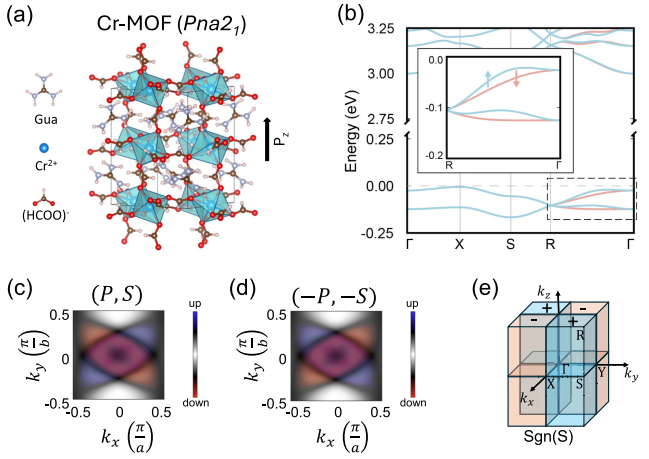

FIG. 2. (a) Crystal structure of Cr-MOF. (b) Spin-split band structure of Cr-MOF. (c) Spin-resolved isoenergy contour ($E = -0.05$ eV) for the (P,S) state at the $k_z = 0.25$ plane, blue and red denote the spectral weight for spin-up and spin-down, respectively. (d) Same as (c), but for the $(-P,-S)$ state. (e) The sign of ΔE_k^S for the valence band maximum in reciprocal space.

Synergistic switch of electric and spin polarizations—Here, a state with the coexistence of polarization $P\,(P//z)$ and altermagnetism S is denoted as the (P,S) state. The SSG operations that map $P \rightarrow -P$ and $S \rightarrow -S$ are analyzed and listed in Fig. S3. While the SSG operations connecting P to $-P$ state can be one of the following—$\{1\|-1\}$, $\{1\|2_{100}\}$, $\{1\|2_{010}\}$, $\{-1\|-1\}$, $\{-1\|2_{100}\}$, and $\{-1\|2_{010}\}$—only three of them map the (P,S) state to the $(-P,-S)$ state, i.e., $\{1\|2_{100}\}$, $\{1\|2_{010}\}$, and $\{-1\|-1\}$. In addition, whether the $(-P,-S)$ state can be experimentally realized upon the application of an electric field, however, depends on the energy barrier between the two phases, which is ultimately governed by the internal atomic displacements during the phase transition.

To search for the reversed polarization state, one needs to consider the hybrid improper ferroelectricity nature that two zone boundary modes (X_1^- and X_4^+) activate the polar distortion. Thus, reversing either of the zone-boundary modes flips the polarization $P \rightarrow -P$, while, reversing both preserves P (see Supplemental Material Sec. III [30]). For simplicity and without loss of generality, we will use these two modes as variables in below.

Figure 3(a) shows the energy landscape of the coupled zone-boundary modes relative to the *Imma* phase. Starting from the energetically favored (P,S) ground state, if the amplitude of X_1^- mode is continuously reduced and eventually reverses its sign, the structure transforms to a $(-P,S)$ state. This transition path, indicated by the purple line in Fig. 3(a), passes through a centrosymmetric *Pnma* phase. The $(-P,S)$ state and the original (P,S) state are related by $\{1\|m_{001}\}$ SSG operation. The energy barrier is about 4 eV per unit cell, as shown in Fig. 3(b). Such a high energy barrier is attributed to the large atomic distortion amplitude (~6.3 Å) along this path, primarily due to the rotation of the guanidinium molecule. In sharp contrast, when the X_4^+ mode is continuously tuned to the reversed amplitude, the transition occurs via a *Pnna* reference phase [orange line in Fig. 3(a)]. This path leads to the $(-P,-S)$ state, connected by $\{1\|2_{100}\}$ SSG operation, with a significantly lower energy barrier of approximately 0.1 eV [Fig. 3(c)], nearly 40 times smaller than that for the *Pnma* path. Thus, the $(P,S) \rightarrow (-P,-S)$ structural

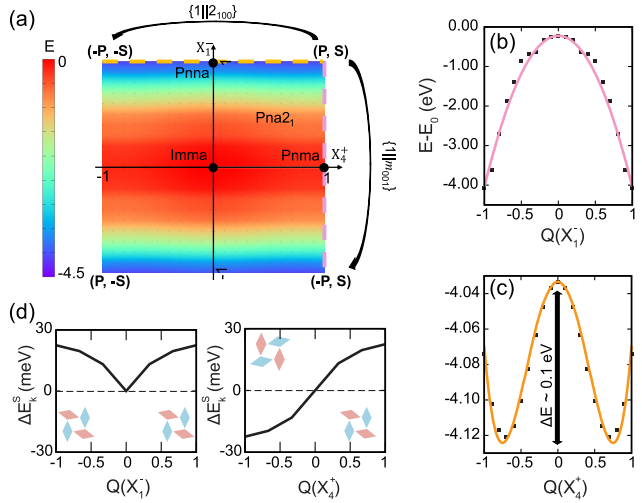

FIG. 3. (a) Energy landscape for the coupling of the X_1^- and X_4^+ modes, where different transition paths are marked by yellow and purple dashed lines. (b) and (c) Energy profiles along the two paths denoted in (a). (d) Spin splitting as a function of mode amplitude. The insets in (d) denote the Q_2 Jahn-Teller (JT) pattern at the endpoints, with the pink and blue diamonds denote the octahedra centered with the spin-up and spin-down Cr, respectively. The octahedra distortion patterns associate to different orbital-ordering states between (P, S) and $(-P, -S)$.

transition through the *Pnna* path is energetically favored and represents a possible realistic transition pathway when the polar direction is flipped by an external electric field.

The spin reversal of the isoenergy contour for the $(-P, -S)$ state shown in Fig. 2(d) strongly supports the possibility to control altermagnetic spin splitting by flipping the ferroelectric polarization in this system. We plot the evolution of ΔE_k^s as a function of the respective mode amplitude during the structural transition in Fig. 3(d). We found that ΔE_k^s reduces to zero at the *Pnma* phase and then regresses to its original value as $Q(X_1^-)$ varies, while changing monotonically with respect to $Q(X_4^+)$. Such behavior arises because ΔE_k^s is odd under $\{1\|2_{100}\}$ but even under $\{1\|m_{001}\}$, consistent with the symmetry presented in Fig. 2(e). Furthermore, the microscopic mechanism of the reversal of the altermagnetic spin splitting by reversing the X_4^+ mode can be understood by the change of the Q_2 Jahn-Teller (JT) distortion pattern, as illustrated in the insets of Fig. 3(d). Since the JT distortion is known to couple with the orbital ordering in oxide perovskites [45] and metal-organic framework systems [46], our results provide a concrete example of how altermagnetism can be entangled with orbital ordering [47], offering new insights into the control of spin splitting through orbital as well as lattice degrees of freedom.

To illustrate the electric-field-controllable altermagnetic tunnel junction device, we consider a prototypical homojunction system proposed in Fig. 1(b), where both the fixed and free layers are composed of Cr-MOF. We evaluate the giant magnetoresistance by the ratio between the density-functional theory-calculated longitudinal conductivity of the spin-up and spin-down channels along the [110] direction [48]. Based on a 184-atom $\sqrt{2} \times \sqrt{2}$ supercell, our results suggest that the maximum giant magnetoresistance rate for this system could reach approximately 53% (see Fig. S5 and Supplemental Material Sec. V [30]), validating the potential of ferroelectric switchable altermagnetism for nonvolatile spintronic devices.

Detection of the switch of altermagnetic spin splitting—The direct experimental detection of the AFM-induced spin splitting typically requires advanced techniques such as spin-resolved angle-resolved photoemission spectroscopy [49,50]. Since the Néel vector remains unchanged through the $(P, S) \rightarrow (-P, -S)$ transition, we propose a way to detect the switch of altermagnetic spin splitting through the linear-polarized photogalvanic spin current effect (spin LPGE), which directly couples to the spin polarization through nonlinear optical response. By using the SSG symmetry analysis implemented in FINDSPINGROUP, we find that six nonzero Berry curvature dipole tensor elements $(D_{xxz}, D_{xzx}, D_{zxx}, D_{yyz}, D_{yzy}, D_{zyy})$ are allowed without SOC in Cr-MOF. All the other tensor elements, such as the quantum metric dipole and inverse mass dipole [51], are forbidden. The nonzero Berry curvature dipole can induce a nonlinear Hall current in transport measurement, as well as the spin LPGE from an optical perspective. Because of the broken spatial inversion symmetry, a shift current is expected under linear-polarized light excitation [52]. In a Cr-MOF system, both charge and spin currents can be generated: the charge current reflects the direction of the electric polarization P, while the spin current serves as a signature of the difference between the two spin channels, i.e., the spin splitting.

The spin LPGE conductivity component $\sigma_{\uparrow-\downarrow}^{zyy}$ for the (P, S) and $(-P, -S)$ states is shown in Fig. 4 (see Supplemental Material Sec. IV [30]). A nonzero dc current begins to emerge when the photon energy exceeds the band gap, reaching the first peak at about 3.2 eV with a value of

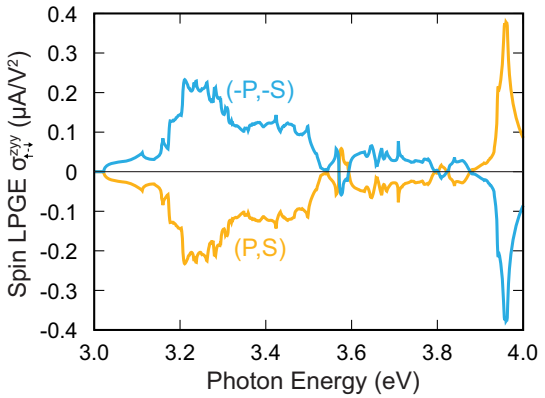

FIG. 4. The spin LPGE conductivity component $\sigma_{\uparrow-\downarrow}^{zyy}$ for the (P, S) and $(-P, -S)$ states.

about 0.23 $\mu A/V^2$. The second peak, near 4 eV, is attributed to the spin splitting at the higher conduction bands. During the $(P, S) \rightarrow (-P, -S)$ structure transition, the sign of the spin LPGE current reverses. Therefore, the spin LPGE current can serve as a signature of the reversal of the altermagnetic spin splitting.

Conclusion and discussion—Recently, the gate-field control of different spin channels in layered altermagnets through a spin-valley-layer locking effect has been proposed [53,54], highlighting the importance for the manipulation of spin degree of freedom in altermagnets. However, such a nonversatile strategy requires the constant application of an external electric field, which is not favorable for storage devices unless further integrated with other materials. Sliding ferroelectricity [55] or phase transition between ferroelectric and antiferroelectric states [56] can also be used to tune the $\mathcal{PT}$ symmetry in the two dimensional van der Waals systems, which eventually control the emergence of the altermagnetic state. Considering that the hybrid improper ferroelectric materials can be artificially designed by chemistry or strain engineering [57], our study provides a wide configuration space for designing versatile ferroelectric switchable altermagnets.

Our approach provides a novel method for controlling spin properties through ferroelectric polarization, which differs from traditional magnetoelectric multiferroics where ferroelectricity is used to control the net magnetic moment. For the Class 1 candidate $Ca_3Mn_2O_7$, the energy splitting ($\sim$100 meV) is even larger than that of Cr-MOF. Spin canting is allowed in this system, leading to a weak net ferromagnetic moment M. Our symmetry analysis shows that the order parameter for spin splitting S follows the same transformation rules as that for M [11], which can be detected by the anomalous Hall effect. Therefore, an additional order parameter M is added to the coupled degrees of freedom, i.e., (P, M, S), offering multiple tuning knobs for material manipulation and providing enhanced versatility in device design (see Supplemental Material Sec. VI [30]). In contrast, for the Class 2 candidates with no net magnetic moment, traditional magnetic detection methods such as the magneto-optical Kerr effect [58] could be effective only as a high order effect [16]. However, our approach still offers a viable pathway to achieve magnetoelectric coupling by correlating the electric polarization with spin splitting in reciprocal space.

Note added—Recently, we became aware of a related study on $Ca_3Mn_2O_7$ for the "altermagnetoelectric effect" [59], a concept similar to the ferroelectric switchable altermagnetism proposed in our work.

Acknowledgments—A. S. acknowledges useful discussions with P. Radaelli (Oxford University), P. Barone (CNR-SPIN), Sang-Wook Cheong (Rutgers University), and Xinfeng Chen (Xi'an Jiaotong University). This work was supported by the National Key R&D Program of China under Grant No. 2019YFA0704900, the National Natural Science Foundation of China under Grants No. 12274194 and No. 12474232, Guangdong Provincial Key Laboratory for Computational Science and Material Design under Grant No. 2019B030301001, Shenzhen Science and Technology Program (Grants No. RCJC20221008092722009 and No. 20231117091158001), the Innovative Team of General Higher Educational Institutes in Guangdong Province (Grant No. 2020KCXTD001), Guangdong Provincial Quantum Science Strategic Initiative under Grant No. GDZX2401002, the Science Technology and Innovation Commission of Shenzhen Municipality (JCYJ20210324104812034), Natural Science Foundation of Guangdong Province (2021A1515110389), and Center for Computational Science and Engineering of Southern University of Science and Technology. This work has also been funded by the European Union–NextGenerationEU, Mission 4, Component 1, under the Italian Ministry of University and Research (MUR) National Innovation Ecosystem grant ECS00000041-VITALITY-CUP B43C22000470005. We also acknowledge the support by bilateral agreement for scientific collaboration CNR and NSFC (China), "Ferroelectric and chiral hybrid organic inorganic perovskites," for the years 2024-2025 (CUP B53C2300716000). K. Y. was supported by an individual grant (No. CG092501) at the Korea Institute for Advanced Study.

[1] H. Schmid, Multi-ferroic magnetoelectrics, Ferroelectrics **162**, 317 (1994).
[2] N. A. Spaldin, Multiferroics: Past, present, and future, MRS Bull. **42**, 385 (2017).
[3] R. Ramesh and N. A. Spaldin, Multiferroics: Progress and prospects in thin films, Nat. Mater. **6**, 21 (2007).
[4] M. Fiebig, T. Lottermoser, D. Meier, and M. Trassin, The evolution of multiferroics, Nat. Rev. Mater. **1**, 16046 (2016).
[5] X.-Z. Lu and J. M. Rondinelli, Design of new multiferroic oxides, *Handbook of Materials Modeling: Applications: Current and Emerging Materials* (Springer, Cham, 2020), p. 1151.
[6] D. Khomskii, Classifying multiferroics: Mechanisms and effects, Physics **2**, 20 (2009).
[7] J. Wang, J. B. Neaton, H. Zheng, V. Nagarajan, S. B. Ogale, B. Liu, D. Viehland, V. Vaithyanathan, D. G. Schlom, U. V. Waghmare, N. A. Spaldin, K. M. Rabe, M. Wuttig, and R. Ramesh, Epitaxial $BiFeO_3$ multiferroic thin film heterostructures, Science **299**, 1719 (2003).
[8] B. B. Van Aken, T. T. M. Palstra, A. Filippetti, and N. A. Spaldin, The origin of ferroelectricity in magnetoelectric $YMnO_3$, Nat. Mater. **3**, 164 (2004).
[9] T. Kimura, T. Goto, H. Shintani, K. Ishizaka, T. Arima, and Y. Tokura, Magnetic control of ferroelectric polarization, Nature (London) **426**, 55 (2003).
[10] M. Mostovoy, Multiferroics: Different routes to magnetoelectric coupling, npj Spintronics **2**, 18 (2024).

[11] N. A. Benedek and C. J. Fennie, Hybrid improper ferroelectricity: A mechanism for controllable polarization-magnetization coupling, Phys. Rev. Lett. **106**, 107204 (2011).
[12] M. Liu, Y. Zhang, L.-F. Lin, L. Lin, S. Yang, X. Li, Y. Wang, S. Li, Z. Yan, X. Wang, X.-G. Li, S. Dong, and J.-M. Liu, Direct observation of ferroelectricity in $Ca_3Mn_2O_7$ and its prominent light absorption, Appl. Phys. Lett. **113**, 022902 (2018).
[13] S. Hayami, Y. Yanagi, and H. Kusunose, Bottom-up design of spin-split and reshaped electronic band structures in antiferromagnets without spin-orbit coupling: Procedure on the basis of augmented multipoles, Phys. Rev. B **102**, 144441 (2020).
[14] L. Šmejkal, J. Sinova, and T. Jungwirth, Emerging research landscape of altermagnetism, Phys. Rev. X **12**, 040501 (2022).
[15] L. Šmejkal, J. Sinova, and T. Jungwirth, Beyond conventional ferromagnetism and antiferromagnetism: A phase with nonrelativistic spin and crystal rotation symmetry, Phys. Rev. X **12**, 031042 (2022).
[16] P. G. Radaelli, Tensorial approach to altermagnetism, Phys. Rev. B **110**, 214428 (2024).
[17] K. Samanta, D.-F. Shao, and E. Y. Tsymbal, Spin filtering with insulating altermagnets, arXiv:2409.00195.
[18] B. Chi, L. Jiang, Y. Zhu, G. Yu, C. Wan, and X. Han, Anisotropic spin filtering by an altermagnetic barrier in magnetic tunnel junctions, Phys. Rev. Appl. **23**, 014013 (2025).
[19] L. Bai, W. Feng, S. Liu, L. Šmejkal, Y. Mokrousov, and Y. Yao, Altermagnetism: Exploring new frontiers in magnetism and spintronics, Adv. Funct. Mater. **34**, 2409327 (2024).
[20] Q. Liu, X. Dai, and S. Blügel, Different facets of unconventional magnetism, Nat. Phys., (2025).
[21] S. V. Gallego, J. M. Perez-Mato, L. Elcoro, E. S. Tasci, R. M. Hanson, K. Momma, M. I. Aroyo, and G. Madariaga, Magndata: Towards a database of magnetic structures. I. The commensurate case, J. Appl. Crystallogr. **49**, 1750 (2016).
[22] A. Stroppa, P. Barone, P. Jain, J. M. Perez-Mato, and S. Picozzi, Hybrid improper ferroelectricity in a multiferroic and magnetoelectric metal-organic framework, Adv. Mater. **25**, 2284 (2013).
[23] K. Yananose, E. R. Clark, P. J. Saines, P. Barone, A. Stroppa, and J. Yu, Synthesis and magnetic properties of the multiferroic $[C(NH_2)_3]Cr(HCOO)_3$ metal–organic framework: The role of spin–orbit coupling and Jahn–Teller distortions, Inorg. Chem. **62**, 17299 (2023).
[24] P. Liu, J. Li, J. Han, X. Wan, and Q. Liu, Spin-group symmetry in magnetic materials with negligible spinorbit coupling, Phys. Rev. X **12**, 021016 (2022).
[25] X. Chen, J. Ren, Y. Zhu, Y. Yu, A. Zhang, P. Liu, J. Li, Y. Liu, C. Li, and Q. Liu, Enumeration and representation theory of spin space groups, Phys. Rev. X **14**, 031038 (2024).
[26] Y. Jiang, Z. Song, T. Zhu, Z. Fang, H. Weng, Z.-X. Liu, J. Yang, and C. Fang, Enumeration of spin-space groups: Toward a complete description of symmetries of magnetic orders, Phys. Rev. X **14**, 031039 (2024).
[27] Z. Xiao, J. Zhao, Y. Li, R. Shindou, and Z.-D. Song, Spin space groups: Full classification and applications, Phys. Rev. X **14**, 031037 (2024).
[28] X. Chen, Y. Liu, P. Liu, Y. Yu, J. Ren, J. Li, A. Zhang, and Q. Liu, Catalog of unconventional magnons in collinear magnets, arXiv:2307.12366.
[29] https://www.findspingroup.com/
[30] See Supplemental Material at http://link.aps.org/supplemental/10.1103/PhysRevLett.134.106802, which includes Refs. [31–42], for notes regarding the materials screening protocol for ferroelectric altermagnets, identification of ferroelectric switchable altermagnets, symmetry analysis for the candidate Cr-MOFs, details of density-functional theory calculations, calculation details for the giant magnetoresistance rate for Cr-MOF as a tunneling junction, and the discussions of $Ca_3Mn_2O_7$ as another candidate.
[31] M. Viswanathan, S. G. Bhat, A. K. Bera, and J. Rodríguez-Carvajal, Neutron diffraction study on the magnetic structure of the promised multiferroic hybrid perovskite $[C(ND_2)_3]Cu(DCOO)_3$ and its centrosymmetric analogues, J. Phys. Chem. C **123**, 18551 (2019).
[32] Y. Inaguma, K. Tanaka, T. Tsuchiya, D. Mori, T. Katsumata, T. Ohba, K.-i. Hiraki, T. Takahashi, and H. Saitoh, Synthesis, Structural transformation, thermal stability, valence state, and magnetic and electronic properties of $PbNiO_3$ with perovskite- and $LiNbO_3$-type structures, J. Am. Chem. Soc. **133**, 16920 (2011).
[33] G. Kresse and J. Furthmüller, Efficiency of ab-initio total energy calculations for metals and semiconductors using a plane-wave basis set, Comput. Mater. Sci. **6**, 15 (1996).
[34] M. Ropo, K. Kokko, and L. Vitos, Assessing the Perdew-Burke-Ernzerhof exchange-correlation density functional revised for metallic bulk and surface systems, Phys. Rev. B **77**, 195445 (2008).
[35] S. L. Dudarev, G. A. Botton, S. Y. Savrasov, C. J. Humphreys, and A. P. Sutton, Electron-energy-loss spectra and the structural stability of nickel oxide: An LSDA + U study, Phys. Rev. B **57**, 1505 (1998).
[36] A. A. Mostofi, J. R. Yates, Y.-S. Lee, I. Souza, D. Vanderbilt, and N. Marzari, wannier90: A tool for obtaining maximally-localised Wannier functions, Comput. Phys. Commun. **178**, 685 (2008).
[37] N. Marzari, A. A. Mostofi, J. R. Yates, I. Souza, and D. Vanderbilt, Maximally localized Wannier functions: Theory and applications, Rev. Mod. Phys. **84**, 1419 (2012).
[38] Q. Wu, S. Zhang, H.-F. Song, M. Troyer, and A. A. Soluyanov, WannierTools: An open-source software package for novel topological materials, Comput. Phys. Commun. **224**, 405 (2018).
[39] J. Ibañez-Azpiroz, S. S. Tsirkin, and I. Souza, *Ab initio* calculation of the shift photocurrent by Wannier interpolation, Phys. Rev. B **97**, 245143 (2018).
[40] G. Pizzi, D. Volja, B. Kozinsky, M. Fornari, and N. Marzari, BoltzWann: A code for the evaluation of thermoelectric and electronic transport properties with a maximally-localized Wannier functions basis, Comput. Phys. Commun. **185**, 422 (2014).

[41] I. Dzyaloshinskii, A thermodynamic theory of "weak" ferromagnetism of antiferromagnetics, J. Phys. Chem. Solids **4**, 241 (1958).
[42] T. Moriya, Anisotropic superexchange interaction and weak ferromagnetism, Phys. Rev. **120**, 91 (1960).
[43] Y. Guo, H. Liu, O. Janson, I. C. Fulga, J. van den Brink, and J. I. Facio, Spin-split collinear antiferromagnets: A large-scale ab-initio study, Mater. Today Phys. **32**, 100991 (2023).
[44] S. Ghosh, D. Di Sante, and A. Stroppa, Strain tuning of ferroelectric polarization in hybrid organic inorganic perovskite compounds, J. Phys. Chem. Lett. **6**, 4553 (2015).
[45] D. Khomskii, Cooperative Jahn–Teller effect and orbital ordering, in *Transition Metal Compounds*, edited by D. I. Khomskii (Cambridge University Press, Cambridge, England, 2014), pp. 204–237.
[46] A. Stroppa, P. Jain, P. Barone, M. Marsman, J. M. Perez-Mato, A. K. Cheetham, H. W. Kroto, and S. Picozzi, Electric control of magnetization and interplay between orbital ordering and ferroelectricity in a multiferroic metal–organic framework, Angew. Chem. Int. Ed. **50**, 5847 (2011).
[47] V. Leeb, A. Mook, L. Šmejkal, and J. Knolle, Spontaneous formation of altermagnetism from orbital ordering, Phys. Rev. Lett. **132**, 236701 (2024).
[48] L. Šmejkal, A. B. Hellenes, R. González-Hernández, J. Sinova, and T. Jungwirth, Giant and tunneling magnetoresistance in unconventional collinear antiferromagnets with nonrelativistic spin-momentum coupling, Phys. Rev. X **12**, 011028 (2022).
[49] J. Krempaský *et al.*, Altermagnetic lifting of kramers spin degeneracy, Nature (London) **626**, 517 (2024).
[50] Y.-P. Zhu *et al.*, Observation of plaid-like spin splitting in a noncoplanar antiferromagnet, Nature (London) **626**, 523 (2024).
[51] H. Zhu, J. Li, X. Chen, Y. Yu, and Q. Liu, Magnetic geometry to quantum geometry nonlinear transports, arXiv:2406.03738.
[52] M. S. Okyay, S. A. Sato, K. W. Kim, B. Yan, H. Jin, and N. Park, Second harmonic Hall responses of insulators as a probe of berry curvature dipole, Commun. Phys. **5**, 303 (2022).
[53] R.-W. Zhang, C. Cui, R. Li, J. Duan, L. Li, Z.-M. Yu, and Y. Yao, Predictable gate-field control of spin in altermagnets with spin-layer coupling, Phys. Rev. Lett. **133**, 056401 (2024).
[54] R. Peng, J. Yang, L. Hu, W.-L. Ong, P. Ho, C. S. Lau, J. Liu, and Y. S. Ang, All-electrical layer-spintronics in altermagnetic bilayer, arXiv:2408.12504.
[55] W. Sun, W. Wang, C. Yang, R. Hu, S. Yan, S. Huang, and Z. Cheng, Altermagnetism induced by sliding ferroelectricity via lattice symmetry-mediated magnetoelectric coupling, Nano Lett. **24**, 11179 (2024).
[56] X. Duan, J. Zhang, Z. Zhang, I. Zutic, and T. Zhou, preceding Letter, Antiferroelectric altermagnets: Antiferroelectricity alters magnets, Phys. Rev. Lett. **134**, 106801 (2025).
[57] D. Puggioni and J. M. Rondinelli, Designing a robustly metallic noncenstrosymmetric ruthenate oxide with large thermopower anisotropy, Nat. Commun. **5**, 3432 (2014).
[58] F.-R. Fan, H. Wu, D. Nabok, S. Hu, W. Ren, C. Draxl, and A. Stroppa, Electric-magneto-optical Kerr effect in a hybrid organic–inorganic perovskite, J. Am. Chem. Soc. **139**, 12883 (2017).
[59] L. Šmejkal, Altermagnetic multiferroics and altermagnetoelectric effect, arXiv:2411.19928.